 FDMP, vol.2, no.28, pp.1-8, 2007

A Deterministic Mechanism for Side-branching in Dendritic Growth

Shuwang Li[1], Xiangrong Li[1], John Lowengrub[1,2] and Martin Glicksman[3]

Abstract: In this paper, we suggest a deterministic mechanism for the generation and development of side-branches in dendritic growth. We investigated the existence of such a mechanism for Gibbs-Thomson-Herring (GTH [1]) anisotropic capillary boundary condition recently in our previous work [2] . Here, we focus our study on the GTH anisotropic kinetic boundary condition. We develop and apply accurate boundary integral methods in 2D and 3D, in which a time and space rescaling scheme, capable of separating the dynamics of growth from those of morphology change, is implemented. Numerical results reveal that under anisotropic kinetic boundary conditions, a non-monotone temperature distribution forms on the interface that leads to oscillations of the scaled tip velocity. This dynamical process works like a limit cycle that generates a sequence of protuberances near the tip. These protuberances propagate away from the tip and develop into side-branches at later times. Unlike the conventional noise-amplification theory [3], the generation and development of side-branches is intrinsic and occurs solely under the influence of GTH boundary condition.

keyword: dendrites, side-branching, solidification, boundary integral.

1 Introduction

Dendrites growing from the supercooled melts or supersaturated solutions are characterized by smooth, parabolic-like tips and side-branches behind the tips. Understanding the formation of dendritic structures has long been a challenging research topic in materials science. Through a combination of analysis, numerics and experiments [3, 4, 5, 6, 7, 8, 9, 10, 11, 12, 13, 14], it is now recognized that anisotropies in surface tension and/or in the atomic attachment kinetics play an important role to stabilize the tip region against tip splitting. The mechanism that determines the generation and development of side-branches, however, remains as a subject of controversy.

The conventional theory for the formation of side-branches, first proposed by Pieters and Langer [3], states that the dendritic side-branches may be generated by selective noise amplification near the tip and the noise may come from the thermal fluctuations in the system. Using a two dimensional boundary-layer model with kinetic crystalline anisotropy, their numerical results and linear asymptotic analysis suggest that a small random perturbation added to the tip velocity can be amplified to form visible side-branches. Measurements of the dendritic growth of NH_4Br crystals from supersaturated solution by Dougherty *et.al* are consistent with the noise amplification proposition in that the observed side-branches on opposite sides of the dendrite are imperfectly correlated and there are variations in both phase and amplitude [9]. These observations agree with the random nature of noise amplification theory though the origin of noise in the experiment remains as an open question.

Using a geometrical model, Martin and Goldenfeld investigated the existence of a deterministic mechanism for the formation of side-branches within the framework of an eigenmode analysis of a linear stability operator [11]. They presented a number of possible reasons for the generation of side-branches in dendritic growth, such as a limit cycle behavior due to a Hopf bifurcation and a solvability-induced side-branching [11]. Their analysis emphasizes the importance of nonlinear effects and suggests that the combination of both nonlinear dynamics and the singular

[1] Department of Mathematics, University of California at Irvine, Irvine CA 92697
[2] Department of Chemical Engineering and Material Science, University of California at Irvine, Irvine CA 92697
[3] Department of Material Science and Engineering,University of Florida, Galnesville, FL 32611

nature of the steady state is responsible for side-branching [11]. Experimental results by Couder *et. al* show that the nonlinear effects play an important role in the generation of side-branching [12, 13]. In these experiments, a small air bubble is placed at the tip of viscous finger in a Hele-Shaw cell. The nonlinear interaction between the small air bubble and the finger tip gives rise to the generation of perfectly correlated side-branches on either side of the finger. This suggests that noise effects are not important here. Similar phenomena were also observed in liquid crystals. Borzsonyi *et. al* [14] demonstrated that by applying a nonlocal periodic force (e.g. an oscillatory pressure or heating) in the vicinity of the liquid crystal dendrite tip, the resulting tip velocity becomes oscillatory and side-branches are regularized by these forces, i.e. the side-branches are nearly perfect-correlated, which indicates that the noise amplification mechanism is not important here either. Using non-Newtonian fluids, Kondic *et. al* [15, 16, 17] found that a shear-rate dependent viscosity of the driven fluid significantly influences pattern formation in a Hele-Shaw cell. In particular, shear thinning suppresses tip-splitting and produces fingers which grow in an oscillating manner, shedding side-branches from their tips. These results again strongly suggest that an oscillatory tip velocity is important to the understanding of the generation and development of side-branches, which was recognized previously in Pieters and Langer's work [3] although with a non-deterministic origin.

The noise amplification theory certainly provides an explanation of side-branching in some systems, but the experimental and theoretical results mentioned above suggest that deterministic mechanisms for side-branching need to be further explored. The existence of such a mechanism for the Gibbs-Thomson-Herring (GTH) anisotropic capillary boundary condition was investigated recently in our previous work [2]. In this paper, we focus our study on an evolving crystal with the Gibbs-Thomson-Herring anisotropic kinetic boundary condition. We develop accurate 2D and 3D boundary integral methods in which a time and space rescaling scheme is implemented in a way such that the area/volume of the crystal keeps unchanged. By scaling out the overall growth of the evolving crystal, we are able to track the detailed dynamics of dendrite tip due to the GTH boundary condition. Our numerical results reveal that the interface can develop a non-monotone temperature distribution that leads to the oscillations of the scaled tip velocity. This dynamical process works like a limit cycle and generates a sequence of protuberances near the tip that propagate away from the tip and form side-branches at later times. Unlike the conventional noise-amplification theory [3], the formation of side-branches is intrinsic and occurs solely under the influence of the GTH boundary condition, without any significant noise present.

This paper is organized as follows: in section 2, we review the governing equations; in section 3, we present the rescaling scheme; in section 4, we discuss numerical results; and in section 5, we give conclusions.

2 Governing Equations

In this paper, we consider a solid crystal growing quasi-statically in a supercooled liquid phase. The interface Σ separates the solid phase Ω_1 from the liquid phase Ω_2. We assume that for simplicity the surface tension along the interface is isotropic, and the interfacial kinetic coefficient is 4-fold anisotropic, i.e. $\varepsilon(\mathbf{n}) = \varepsilon_0(1-\beta\left(3-4\left(n_1^2+n_2^2+n_3^2\right)\right))$ where n_i denote the components of the normal vector $\mathbf{n}$. In 2D, this reduces to $\varepsilon(\theta) = (1+\mu\cos(4\theta))$, where θ is the angle between the normal vector and a fixed axis, and μ represents the strength of anisotropy. For simplicity, the thermal diffusivities of the two phases are assumed to be identical. The length scale is the equivalent radius of the crystal (radius of a sphere/circle with the same volume/area) at time $t = 0$ and the time scale is the characteristic surface tension relaxation time scale [19, 20, 21]. The following non-dimensional equations govern the growth of the crystal:

$$\nabla^2 T_i = 0 \qquad \text{in } \Omega_i \qquad \text{i=1,2,} \tag{1}$$

$$V = (\nabla T_1 - \nabla T_2)\cdot \mathbf{n} \qquad \text{on } \Sigma, \tag{2}$$

$$T_1 = T_2 = -\kappa - \varepsilon(\mathbf{n})V \qquad \text{on } \Sigma, \tag{3}$$

$$J = \frac{1}{2(N-1)\pi}\int_\Sigma V d\Sigma, \tag{4}$$

where T_i is the temperature field, $i = 1$ for solid phase and $i = 2$ for liquid phase, κ is the mean curvature, and J is the integral far-field heat flux and specifies the time derivative of the volume/area of the solid phase and $N = 2, 3$ is the spatial dimension. In this paper, $J = C \cdot R(t)^{N-2}$ where R is the equivalent radius at time t and C is a constant. The interface Σ evolves via

$$\mathbf{n} \cdot \frac{d\mathbf{x}}{dt} = V \qquad \text{on } \Sigma, \tag{5}$$

where V is the normal velocity of the interface and $\mathbf{n}$ is the unit normal directed towards Ω_2.

Equation (3) is the well known anisotropic kinetic GTH boundary condition. The kinetic coefficient reflects the underlying crystallographic orientation (4-fold cubic symmetry) and represents the finite rate of atomic attachment from the liquid phase to the solid phase. A non-zero, anisotropic interfacial kinetic coefficient causes the interface to deviate from its local equilibrium temperature and introduces preferred growth directions.

Since the temperature fields in both solid and liquid phases are harmonic, the temperature may be given as a single-layer potential. This yields the second-kind Fredholm integral equations [23] for $V(\mathbf{x})$ and $T_\infty(t)$ where the latter is the far-field temperature. This gives,

$$-\kappa(\mathbf{x}) - \varepsilon(\mathbf{n})V = \int_\Sigma G(\mathbf{x}-\mathbf{x}')V(\mathbf{X}')d\Sigma(\mathbf{x}') + T_\infty \tag{6}$$

$$J = \frac{1}{2(N-1)\pi}\int_\Sigma V(\mathbf{x}')d\Sigma(\mathbf{x}'), \tag{7}$$

where $G(\mathbf{x}) = \frac{1}{2\pi}\log|\mathbf{x}|$ in 2D and $G(\mathbf{x}) = \frac{1}{4\pi}1/|\mathbf{x}|$ in 3D are the Green's functions.

3 Time and space rescaling scheme

In order to accurately and efficiently simulate the nonlinear dynamics of the evolving crystal, we use 2D and 3D boundary integral methods in which a time and space rescaling is implemented. The methods are capable of separating the dynamics of growth from those of morphology change. This enables us to capture the processes underlying side-branching. We have successfully implemented this scheme to study the long time dynamics of a growing crystal [18, 20, 21] and viscous fingering in a Hele-Shaw cell [22]. For completeness, the method is briefly described below. We introduce the following spatial and temporal scaling

$$\mathbf{x} = \overline{R}(\bar{t})\overline{\mathbf{x}}(\bar{t},\alpha), \tag{8}$$

$$\bar{t} = \int_0^t \frac{1}{\rho(t')}dt', \tag{9}$$

where $\overline{R}(\bar{t}) = R(t(\bar{t}))$ and $\overline{\mathbf{x}}(\bar{t},\alpha)$ is the position vector of the scaled interface, and $\bar{t}$ is the new time variable and ρ defines the new time scale. The scaling $\overline{R}$ is chosen such that the volume $\overline{Vol}$ in 3D and area $\overline{A}$ in 2D enclosed by the scaled interface is constant in time. The scaling $\overline{R}$ can be found by integrating the normal velocity over the interface to get

$$\frac{d\overline{R}(\bar{t})}{d\bar{t}} = \frac{\overline{\rho}(\bar{t})}{\overline{R}(\bar{t})^{N-1}\cdot\overline{Vol}}\cdot\frac{2(N-1)\pi}{N}\cdot\overline{J}(\bar{t}) \tag{10}$$

where $\overline{\rho}(\bar{t}) = \rho(t(\bar{t}))$ and analogously $\overline{J}(\bar{t}) = J(t(\bar{t}))$. To achieve exponential growth of $\overline{R}$ in the scaled frame, we choose $\overline{\rho} = \dfrac{\overline{R}^N\overline{vol}N}{2(N-1)\pi\overline{J}}$ following Eq. (10).

The normal velocity in the new frame is $\overline{V}(\bar{t},\alpha) = \dfrac{d\overline{\mathbf{x}}(\bar{t},\alpha)}{d\bar{t}}\cdot\mathbf{n}$ and satisfies

$$-\overline{\kappa}\frac{\overline{\rho}}{\overline{R}^3} - \frac{\varepsilon(\mathbf{n})}{\overline{R}}\overline{\mathbf{x}}\cdot\mathbf{n} - \mathcal{G}[\overline{x}] \quad = \quad \int_{\overline{\Sigma}} G(|\overline{\mathbf{x}}-\overline{\mathbf{x}}'|)\overline{V}ds' + \frac{\varepsilon(\mathbf{n})}{\overline{R}}\overline{V} + \overline{T}_\infty(\bar{t}), \tag{11}$$

and

$$0 = \int_{\overline{\Sigma}} \overline{V} ds, \tag{12}$$

where $\overline{\kappa} = \overline{R}\kappa$ and the scaling factor $\overline{R}$ is

$$\overline{R}(\overline{t}) = \exp(\overline{t}). \tag{13}$$

Further, in Eq. (11) we have taken $\overline{T}_\infty(\overline{t}) = \dfrac{\overline{A}\log(\overline{R})}{\pi} + \dfrac{\overline{\rho}}{\overline{R}^2} T_\infty(t(\overline{t}))$ in 2D and $\overline{T}_\infty(\overline{t}) = \overline{\rho}T^\infty/\overline{R}^2$ in 3D, and $\mathcal{G}(\overline{\mathbf{x}}) = \int_{\overline{\Sigma}} \overline{\mathbf{x}}' \cdot \mathbf{n}(\overline{\mathbf{x}}') G(\overline{\mathbf{x}} - \overline{\mathbf{x}}') ds'$.

To evolve the interface numerically, Eqs. (11) and (12) are discretized in space and solved efficiently using GMRES [25]. In 2D, Eqs. (11) and (12) are discretized in space using spectrally accurate discretizations [24]. The resulting discrete system is solved efficiently using a diagonal preconditioner in Fourier space [24, 26].

In 3D, the surface is discretized using an adaptive surface triangulated mesh [27]. The surface is then divided into three regions[28]: (1) a singular region which contains all the triangles with the evaluation point $\mathbf{x}$ as a vertex; (2) a quasi-singular region which is the collection of triangles whose center is a distance d from $\mathbf{x}$; and (3) a nonsingular region which contains all other triangles. In the non-singular region, the trapezoid rule is used to perform the integration. In the quasi-singular region, a seven-point Gaussian quadrature is used. In the singular region, Duffy's transformation is used to map the triangle to a unit square which removes the $1/r$ singularity and a seven-point Gaussian quadrature is then used. The discretized equations are solved using GMRES with a diagonal preconditioner. The curvature is approximated using a least-squares parabolic fit of the surface [29].

Once $\overline{V}$ is obtained, the interface is evolved by using a second order accurate non-stiff updating scheme in time and the equal arclength parameterization [24, 26] in 2D and an explicit second order Runge-Kutta method in 3D [18, 28].

4 Results

In order to isolate the effects of anisotropic kinetics on the formation of dendrite primary arms and side-branches, the initial crystal shape was chosen to be a unit circle or sphere.

4.1 2D simulations

We consider a small anisotropy coefficient of $\varepsilon(\theta) = 0.16(1 + 0.025\cos(4\theta))$. The crystal is grown under the driving force of a constant far-field heat flux. Because of the symmetry of initial data, the interfacial contours of only one-half of the interface are shown in the sequence of interface morphologies in Fig. 1 and 2. The pattern is clearly dendritic at later times. Because the surface tension is isotropic, this pattern develops solely under the influence of the anisotropic kinetics. Refinement studies (not shown) indicate there is no significant noise present. This is due to the fact that our method is spectrally accurate and that the heat flux used is well below that for which noise due to discretization and rounding errors could be significantly amplified during the computation.

The details of how a side-branch is initiated and grows can be seen in Figs. 1 and 2. In Fig. 1, the scaled tip velocity $\overline{V}$ of the x-primary arm in the scaled frame is shown as a function of $R(t)$; the true tip velocity V is shown as an inset. From Fig. 2, it is seen that during the oscillation, the local maxima in $\overline{V}$ correspond very well with the development of non-monotonic temperature distributions near the tip and the initiation of side-branches. Notice that these oscillations are not observable in the true tip velocity as they are concealed by the overall growth dynamics. Thus, an accurate numerical method, capable of separating the dynamics of growth from those of shape change, is necessary to capture this phenomena.

In Fig. 2[a]-[f], a sequence of interface morphologies and associated interface temperature distributions are shown, corresponding to the index marked along the $\overline{V}$ curve in Fig. 1. In the absence of externally imposed noise or disturbances, the interface develops negative curvature in synchrony with the interfacial temperature becoming non-monotone near the tip. The observed non-monotonicity of the temperature near the tip is periodic, which suggests

the operation of a limit cycle, rather than selective amplification of noise, introduces the formation of dendritic side-branching. The operation of the dendritic limit cycle involves progressive shape changes near the tip that eventually induce a non-monotonic temperature distribution. This leads to the development of a protuberance, changes in the sign of the interface curvature and the formation of a side-branch as seen in Fig. 2[a]-[f]. The cycle then repeats to produce another side-branch.

The initial circular shape, Fig. 2[a], has a a monotonic temperature distribution as the tip is approached ($\alpha \to 0^{\pm}$). In Fig. 2[b] the circular shape becomes curved, and the interfacial temperature distribution changes correspondingly. In Fig. 2[c], a pair of local temperature maxima develop near $\alpha \approx 0.1$. The primary arm of the dendrite along x-axis is about to form. In Fig. 2[d], a primary arm of the dendrite has already formed and negative curvature develops around $\alpha \approx 0.05$. The temperature distribution is about to become non-monotonic. In Fig. 2[e], although it is not apparent yet from the interface at the resolution shown, the interface curvature develops oscillations near the local temperature maxima (around $\alpha \approx 0.05$) that give rise to a small protuberance that will later grow into a side branch. In Fig. 2[f], the small protuberance is now seen. The new local maxima in the temperature near $\alpha 0.05$ are more apparent and the temperature around the tip (from $\alpha = 0.$ to $\alpha \approx \pm 0.05$ becomes monotone again. As can be inferred from Fig. 2[g], new local maxima in the temperature occur and new protuberances will be produced. In Fig. 2[h], we show the small protuberance develops into a side-branch. This completes a limit cycle. This cycle is repeated indefinitely as suggested by the overall solidification pattern.

4.2 3D simulations

In 3D, the results are qualitatively similar to those obtained in 2D when the flux $\overline{J} = C\overline{R}$, where C is a constant. In Figures 3 and 4, results are presented using an initially spherical crystal with anisotropic kinetic coefficient, $\varepsilon(\mathbf{n}) = \varepsilon_0(1-\beta(3-4[n_1^2+n_2^2+n_3^2]))$, $\varepsilon_0 = 0.1$ and anisotropy $\beta = 0.1$. In Figure 3, the scaled velocity, $\overline{V}$, at the tip and the unscaled (true) tip velocity, V, are also shown. As in the two dimensional case, there are oscillations of $\overline{V}$, which suggest the presence of a limit cycle that gives rise to the formation of side-branches. In Figure 4 the crystal morphologies are shown during the evolution (the last frame shows the adaptive mesh). As in 2D, the primary arms form followed by a succession of side-branches whose origin corresponds to the oscillations observed in the normal velocity which arise through a non-monotonic temperature distribution near the tip (not shown).

5 Conclusion and discussion

In this paper, we investigated the existence of a deterministic mechanism for side-branching in dendritic growth under the Gibbs-Thomson-Herring (GTH) anisotropic kinetic boundary condition. We developed accurate 2D and 3D boundary integral methods in which a time and space rescaling scheme is implemented in a way such that the area/volume of the crystal keeps unchanged. By scaling out the overall growth of the evolving crystal, we were able to track the detailed dynamics of dendrite tip due to the GTH boundary condition. Our numerical results revealed that the interface can develop a non-monotone temperature distribution that leads to the oscillations of the scaled tip velocity that apparently acts like a limit cycle and generates a sequence of protuberances near the tip that propagate away from the tip and form side-branches at later times. The formation of side-branches is intrinsic and occurs solely under the influence of the GTH boundary condition, without any significant noise present.

Similar phenomena were observed in our previous work [2], in which the competing anisotropies of the shape and of the surface energy were investigated with regard to the development of side-branching. In [2], a careful analysis of the Gibbs-Thomson-Herring (GTH) boundary condition shows that the combination of shape anisotropy, i.e., an elongated shape in one spatial direction, with surface energy anisotropy can also lead to non-monotone equilibrium temperature distributions. As in the results presented here, a sequence of non-monotonicities in temperature occurs close to the tip, and the temperature field interacts dynamically with the evolving shape. It appears that each time local temperature maxima occur, curvature oscillations develop slightly aft of the tip. These curvature oscillations stimulate the formation of a pair of protuberances, which in most cases continue to grow and form opposing, coherent

side branches.

Though the circular shape used in this paper is not dendritic initially, the anisotropic interfacial kinetics drives the interface to evolve along its preferred direction and the primary arms of the dendrite forms accordingly. A detailed analysis of the coupling between temperature distribution and interface morphologies shows that the mechanisms for side-branching are very similar to what we observed in [2]. The pattern formation mechanism uncovered here and [2] rely solely on the GTH boundary condition. Other interesting morphological phenomena concerning the directional solidification of alloys, such as the cell-to-dendrite transition, and the relationship of side branch spacings to the solidification parameters might also require re-interpretation based on the non-monotonic behavior of the GTH boundary condition disclosed herein.

Experimental observations, such as accomplished in the IDGE, seldom reveal coherent side branching, but this fact might simply be caused by the fact that the thermal fields during dendritic growth are never perfectly symmetrical about the growth axis. Also, what seems especially significant about these simulations of dendritic pattern formation is that perturbations to the crystal-melt interface, and selective amplification of noise, play no role in the process. The GTH boundary condition itself seems to provide a deterministic boundary condition that, when combined with sufficient shape and energy anisotropies, is fully capable of inducing a dynamic limit cycle near the tip. The origin of dendritic side branching might be quite different from current conventional concepts.

Acknowledgement: JSL, XL and SL acknowledge support from the National Science Foundation (DMS) and the generous computing resources from the Network and Academic Computing Services at University of California at Irvine (NACS) and computing resources of BME department (U.C. Irvine). MEG is grateful for his support provided through the John Tod Horton Distinguished Professorship of Materials Science and Engineering when he was in RPI. Thanks are also extended to the National Aeronautics and Astronautics Administration, NASA, Washington, DC, for their financial and operational support of the Isothermal Dendritic Growth Experiment (IDGE).

References

[1]**Herring, C.,** (1951): *Physics of powder metallurgy*, Eds. W.E. Kingston, McGraw-Hill, New York, pp. 143

[2]**Glicksman, M., Lowengrub, J. and Li, S.,** (2006): Non-monotone temperature boundary conditions in dendritic growth, *Proc. in Modelling of Casting, Welding and Adv. Solid. Processes XI.*, Eds. C.A. Gandin and M. Bellet, pp. 521-528

[3]**Pieters, R. and Langer, J.,** (1986): Noise-driven sidebranching in the Boundary-Layer model of dendritic solidification, *Phys. Rev. Lett.* vol.56, pp. 1948-1951

[4]**Jacob, E. and Garik, P.,** (1990): The formation of patterns in non-equilibrium growth, *Nature* vol.343, pp. 523-530

[5]**Glicksman, M., Schaefer, R. and Ayers, J.,** (1976): Dendritic growth–test of theory, *Metall. Trans. A* vol.7, pp. 1747

[6]**Nash, G. and Glicksman, M.,** (1974): Capillarity-limited steady-state dendritic growth–I. theoretical development, *Acta Metall.* vol.22, pp. 1283

[7]**Nash, G. and Glicksman, M.,**(1974): Capillarity-limited steady-state dendritic growth–II. numerical results, *Acta Metall.* vol.22, pp. 1291

[8]**Ihle, T.,** (2000): Competition between kinetic and surface tension anisotropy in dendritic growth, *The Euro. Phys. Journal B* vol.16, pp. 337-344

[9]**Dougherty, A., Kaplan, P., and Gollub, J.,** (1987): Development of side branching in dendritic crystal growth, *Phys. Rev. Lett.* vol.58, pp. 1652-1655

[10]**Karma,A. and Rappel, W.,** (1999): Phase-field model of dendritic sidebranching with thermal noise, *Phys. Rev. E* vol.60, pp. 3614-3625

[11]**Martin, O. and Goldenfeld, N.,** (1987): Origin of sidebranching in dendritic growth, *Phys. Rev. A* vol.35, pp. 1382-1390

[12]**Couder, Y., Cardoso, O., Dupuy, D., Tavernier, P. and Thom, W.,** (1986): Dendritic growth in the Saffman-Taylor experiment, *Euro. Phys. Lett.* vol. 2, pp. 437-443

[13]**Couder, Y., Gerard, N. and Rabaud, M.,,** (1986): Narrow fingers in the Saffman-Taylor instability, *Phys. Rev. A* vol. 34, pp.5175-5178

[14]**Borzsonyi, T., Toth-Katona, T. Buka, A. and Granasy L.,** (2000): Regular dendritic patterns induced by nonlocal time-periodic forcing, *Phys. Rev. E* vol.62, pp. 7817-7827

[15]**Kondic, L., Palffy-Muhoray, P. and Shelley, M.,** (1996): On models of Non-Newtonian Hele-Shaw flow, *Phys. Rev. E* vol.54, pp. 4536-4539

[16]**Kondic, L., Palffy-Muhoray, P. and Shelley, M.,** (1997): Non-Newtonian Hele-Shaw flow and the Saffman-Taylor instability, *Phys. Rev. Lett.* vol.80, pp. 1433-1436

[17]**Fast, P., Kondic, L., Palffy-Muhoray, P. and Shelley, M.,** (2001): Pattern formation in non-Newtonian Hele Shaw flow , *Phys. fluid* vol.13, pp. 1191-1212

[18]**Cristini, V. and Lowengrub, J.,** (2004): Three-dimensional crystal growth- II. Nonlinear simulation and control of the Mullins-Sekerka instability, *J. Crystal Growth* vol. 266, pp. 552-567.

[19]**Li, S., Lowengrub, J. Leo, P. and Cristini, V.,** (2004): Nonlinear theory of self-similar crystal growth and melting, *J. Cryst. Growth* vol. 267, pp. 703-713

[20]**Li, S., Lowengrub, J. Leo, P. and Cristini, V.,** (2005): Nonlinear stability analysis of self-similar crystal growth: control of the MullinsSekerka 424 instability, *J. Cryst. Growth* vol. 277, pp. 578-592

[21]**Li, S., Lowengrub, J. and Leo, P.,** (2005): Nonlinear morphological control of growing crystals , *Physica D* vol. 208, pp. 209-219

[22]**Li, S., Lowengrub, J. and Leo, P.,** (2007): A rescaling scheme with application to the long time simulation of viscous fingering in a Hele-Shaw cell, *J. Comp. Phys.* in press

[23]**Mikhlin, S.,** (1957): Integral equations and their applications to certain problems in mechanics, mathematical physics and Technology, Pergamon, New York

[24]**Hou, T., Lowengrub, J. and and Shelley, M.,** (1994): Removing the stiffness from interfacial flows with surface tension, *J. Comp. Phys.* vol. 114, pp 312-338

[25]**Saad, Y. and Schultz, M.,** (1986): GMRES: a generalized minimal residual algorithm for solving nonsymmetric linear systems, *SIAM J. Sci. Stat. Comput.* vol. 7, pp 856-869.

[26]**Jou, H., Leo, P. and Lowengrub, J.,** (1997): Microstructural evolution in inhomogeneous elastic media, *J. Comp. Phys.* vol. 131, pp 109-148

[27]**Cristini, V., Blawzdziewicz, J. and Loewenberg, M.,** (2001): An adaptive mesh algorithm for evolving surfaces: Simulations of drop breakup and coalescence, *J. Comp. Phys.* vol. 168, pp. 445-463.

[28]**Li, X., Cristini, V., Nie, Q. and Lowengrub, J.,** (2007): Nonlinear three-dimensional simulation of solid tumor growth, *Discrete Dyn. Sys. B* vol. 7, pp. 581-604.

[29]**Zinchenko, A.Z., Rother, M.A., and Davis, R.H.** (1997): A novel boundary integral algorithm for viscous interaction of deformable drops, *Phys. Fluids* vol. 9, pp. 1493-1511.

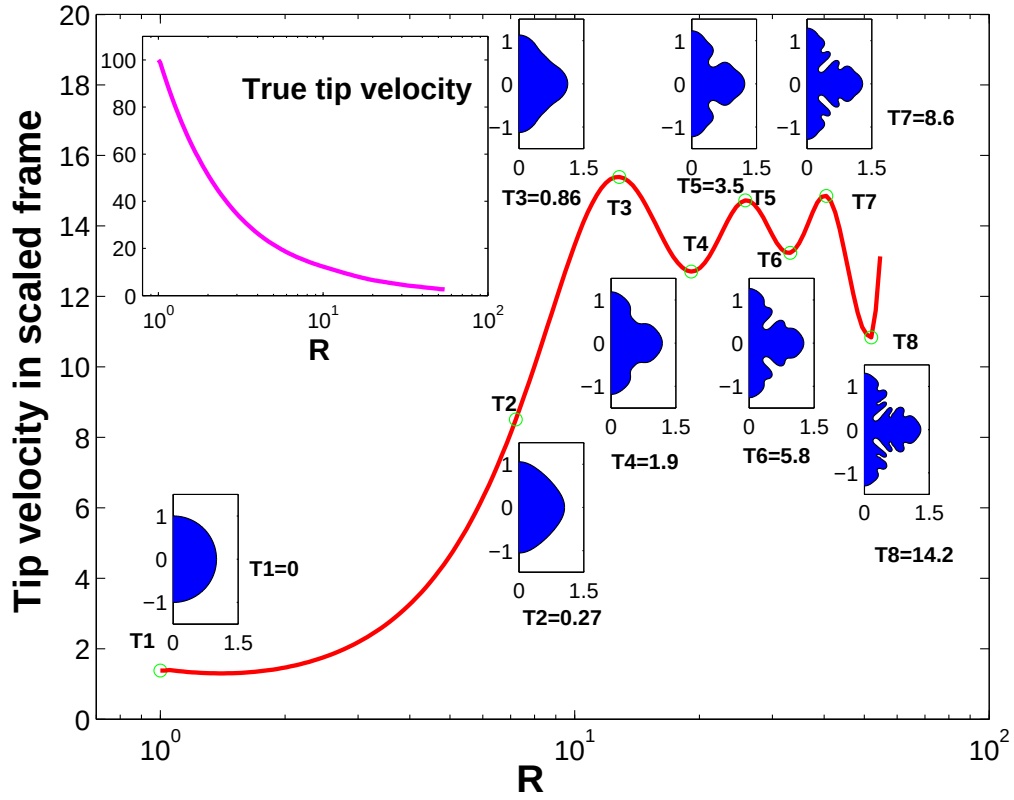

Figure 1 : Boundary integral simulation of the evolution of a circular interface with a kinetics anisotropy of $\varepsilon(\theta) = 0.16(1+0.025cos(\theta))$ and a constant far-field heat flux. The scaled velocity, $\overline{V}$, at the tip and the unscaled (true) tip velocity, V, are also shown. The evolution periodically generates side-branches when the temperature distribution near the tip becomes non-monotonic. These are reflected in the oscillations of $\overline{V}$. The tip grows faster than the surrounding interface, and subsequent negative curvatures are initiated at various locations along the interface where the temperature periodically becomes non-monotonic, suggestive of a dynamic limit cycle.

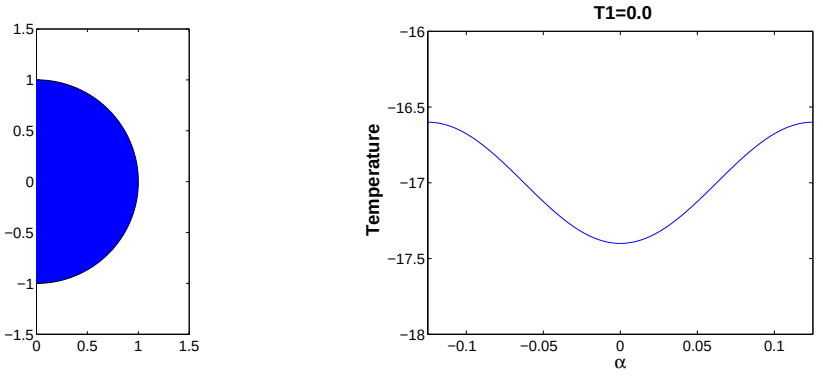
T1=0.0
Temperature
α

[a]

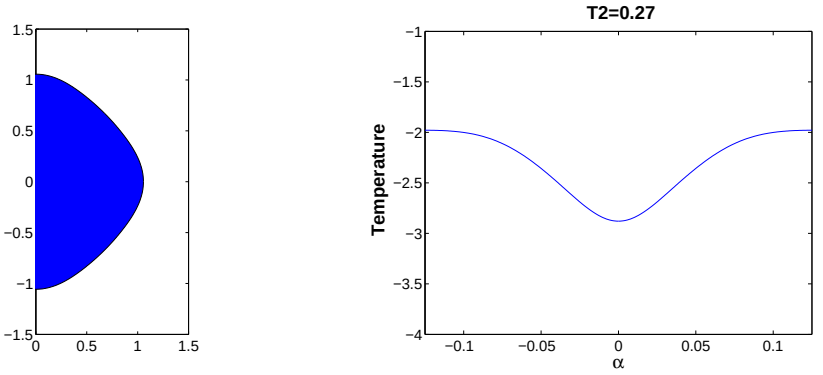
T2=0.27
Temperature
α

[b]

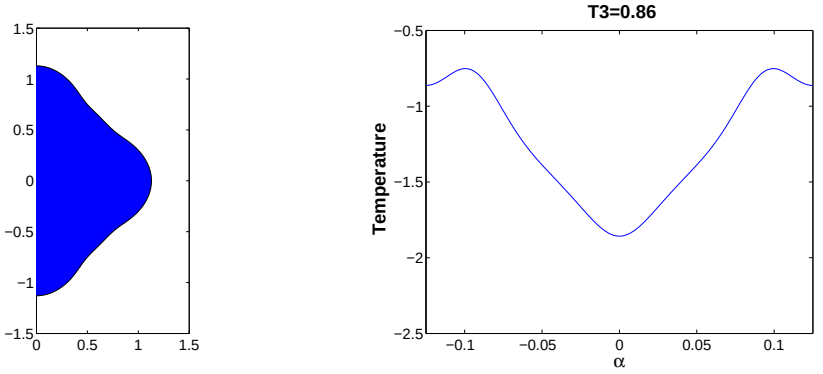
T3=0.86
Temperature
α

[c]

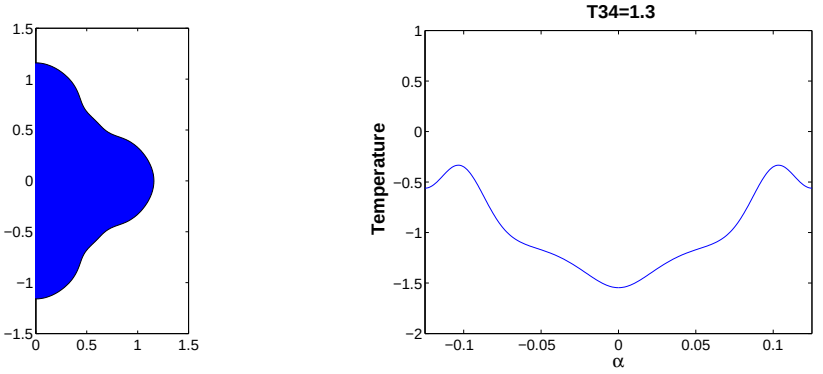
T34=1.3
Temperature
α

[d]

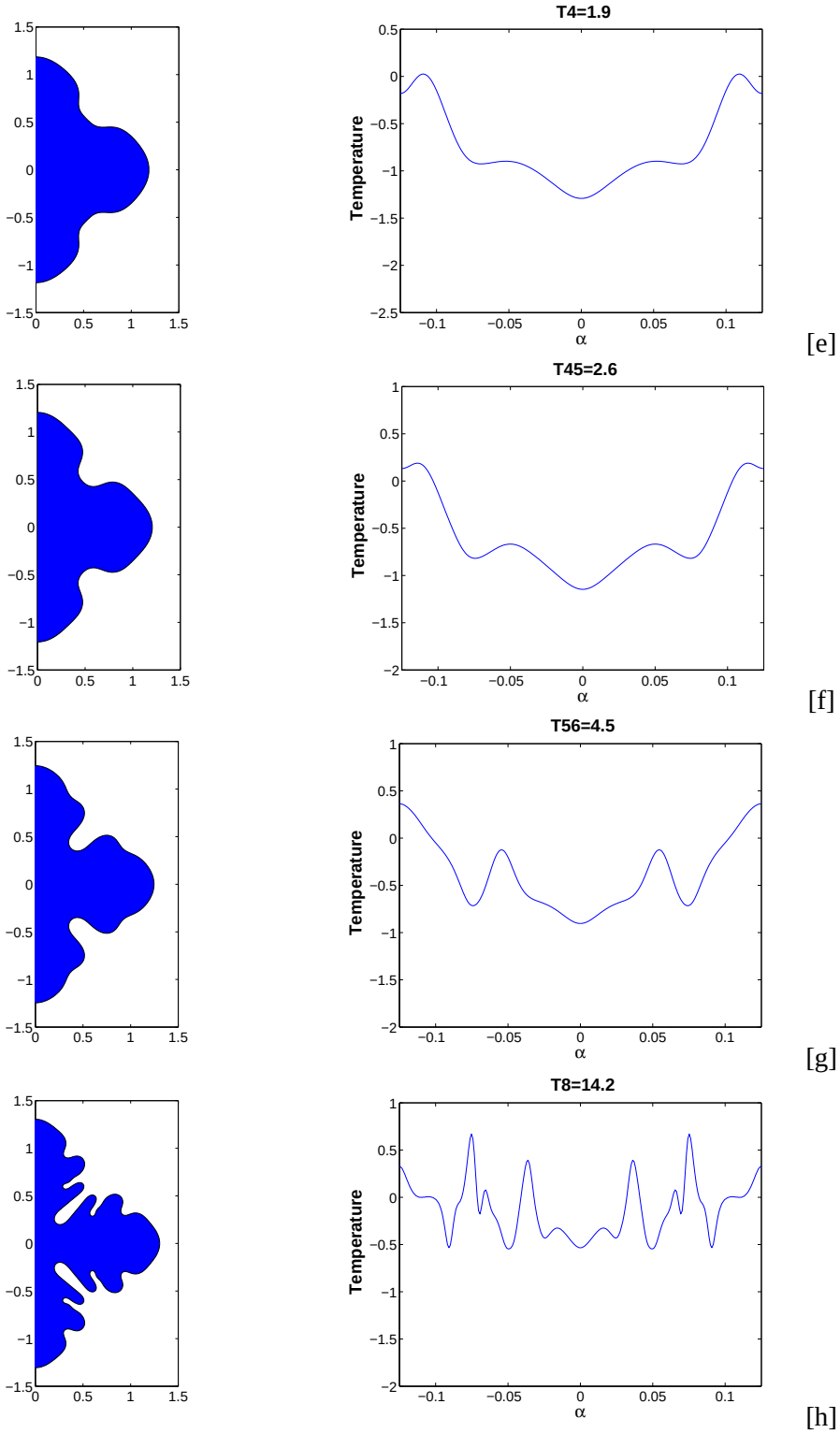

Figure 2 : Details of the development of side branches during evolution of the initially circular interface shown in Fig. 1, suggestive of the operation of a limit cycle. [a] T1 = 0: Starting from a circle, with a monotone-down interface temperature as the tip, $\alpha \rightarrow 0^{\pm}$ is approached. [b] T2 = 0.27: Shape becomes non-circular and a primary arm starts to form. [c] T3 = 0.86: maxima in the temperature develop near $\alpha = 0.1$. Dendrite tip forms. [d] T34 = 1.3: The temperature becomes non-monotone around $\alpha = 0.05$. [e] T4 = 1.9: and [f] T45 =2.6: Negative curvatures form ahead of the growing protuberances, and additional new temperature maxima develops near $\alpha = 0.05$. A pair of protuberance forms. [g] T=5.8, the protuberances develop into side-branches. The temperature near the tip becomes monotonic.

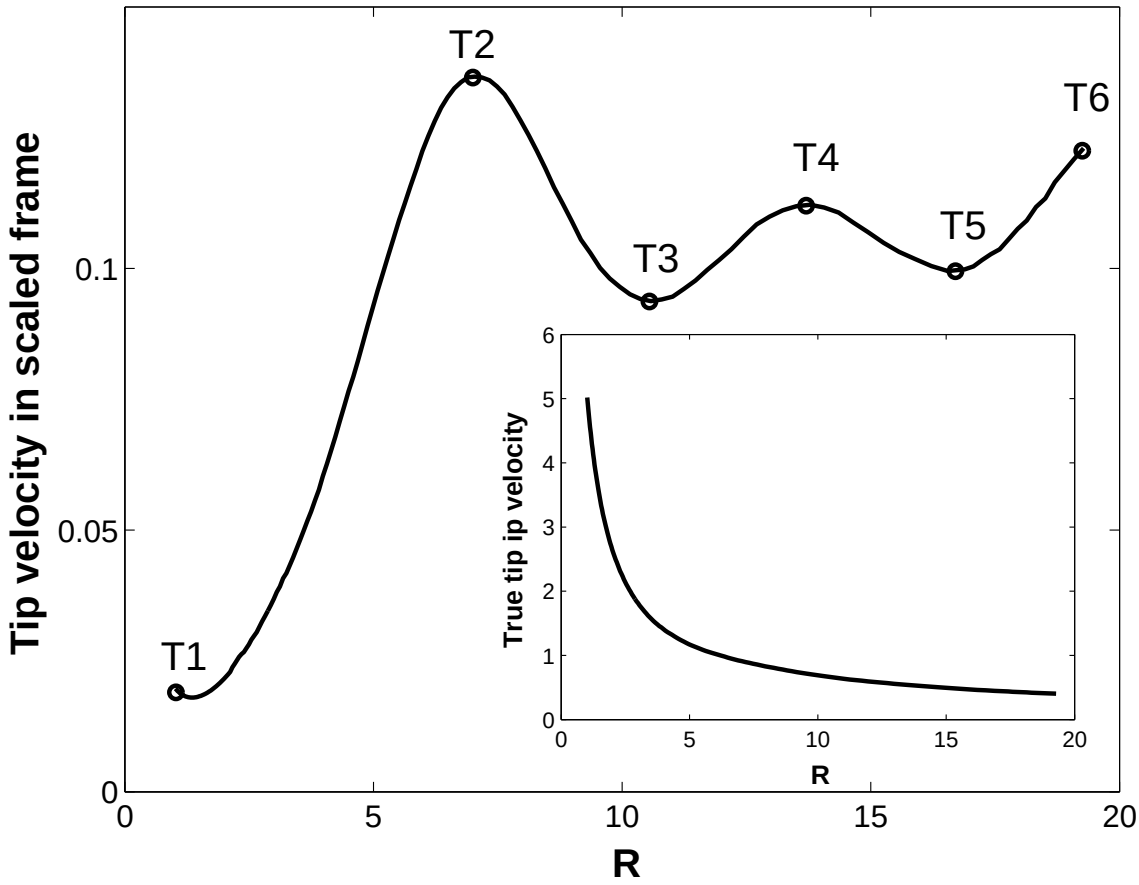

Figure 3 : Three dimensional boundary integral simulation of the evolution of a sphere interface with a far-field heat flux increasing linearly in $R(t)$. The anisotropic kinetic coefficient, $\varepsilon(\mathbf{n}) = \varepsilon_0(1-\beta(3-4[n_1^2+n_2^2+n_3^2]))$, where $\mathbf{n}$ is the outwards normal of the interface with three components n_1, n_2 and n_3, $\varepsilon_0 = 0.1$ and anisotropy $\beta = 0.1$. The scaled velocity, $\overline{V}$, at the tip and the unscaled (true) tip velocity, V, are also shown. Similar to the two dimensional case, there are oscillations of $\overline{V}$, suggest a dynamic limit cycle that gives rise to the formation of side-branches as shown in the following sequence of morphologies.

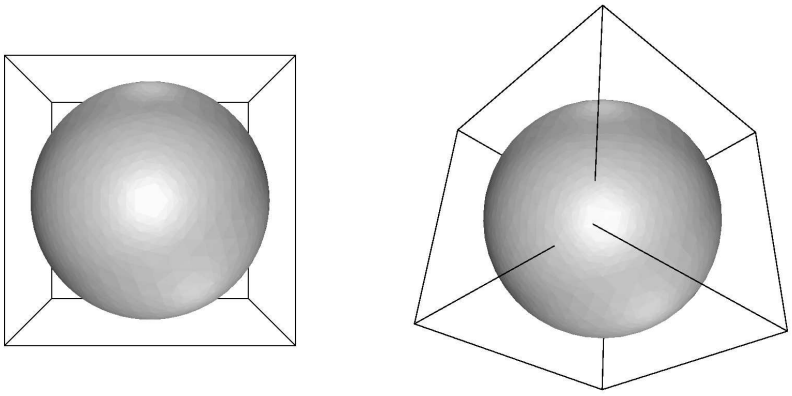

[R=1.0]

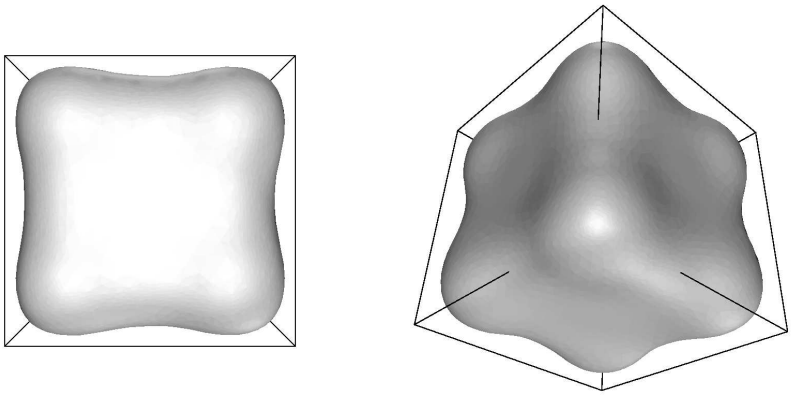

[R=7.0]

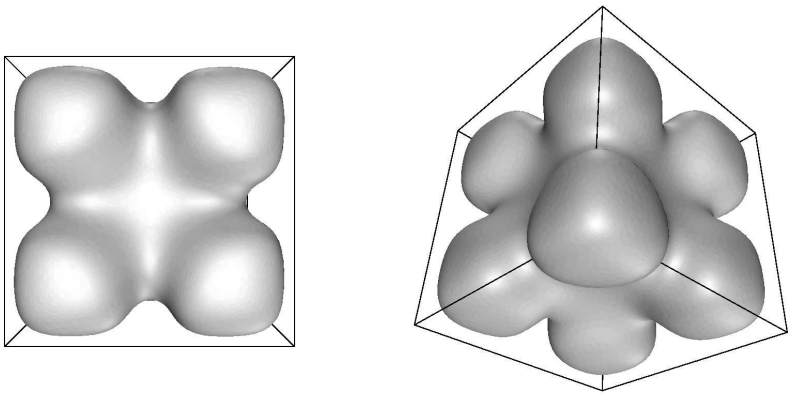

[R=10.6]

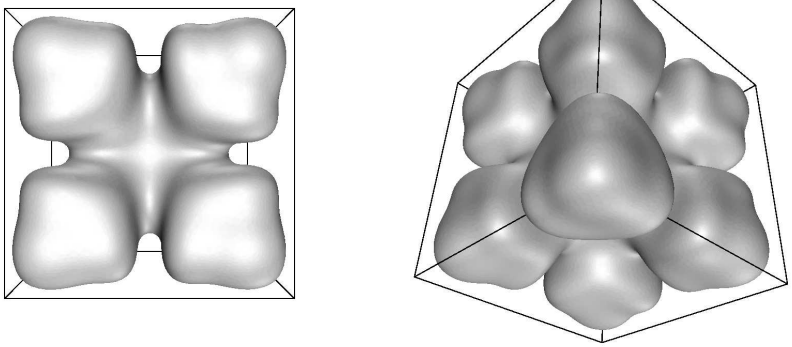

[R=13.7]

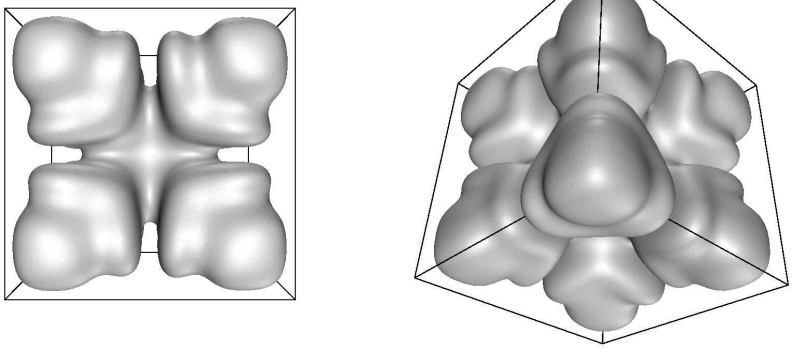

[R=16.07]

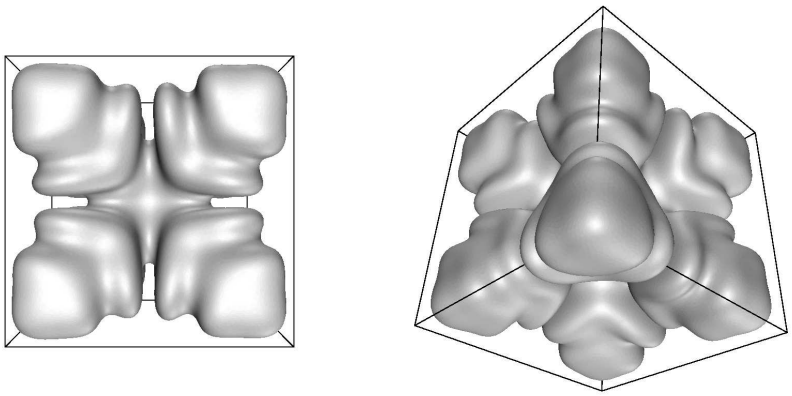

[R=19.3]

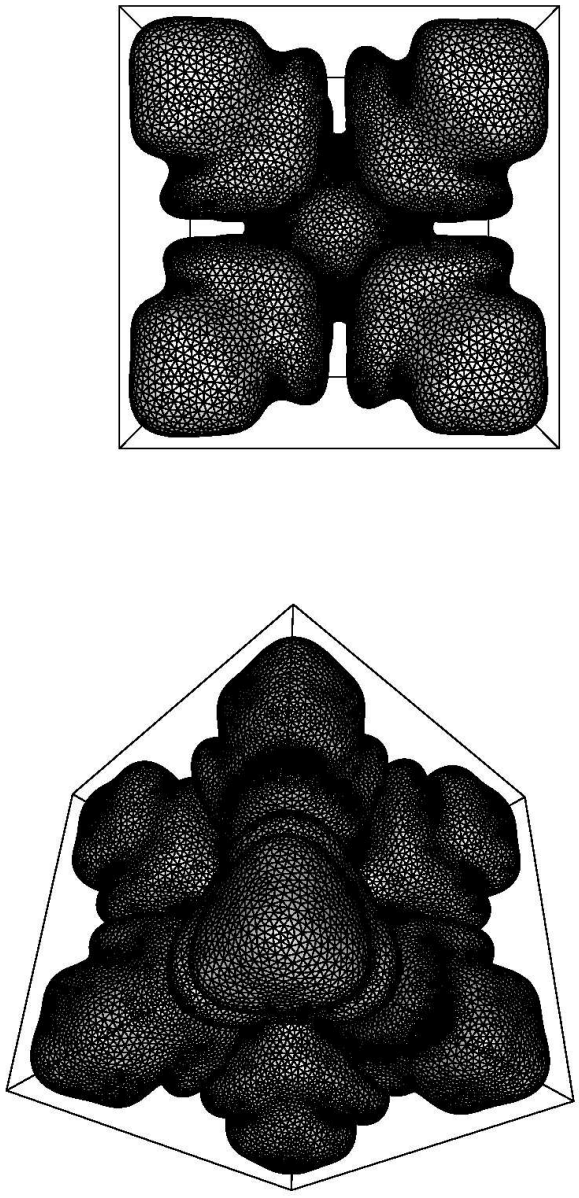

[R=19.3]

Figure 4 : Details of the development of side branches during evolution of a sphere interface with a far-field heat flux increasing linearly in $R(t)$. The number of points $N = 362$ initially and $N = 29,280$ at the final image shown.